Implementation, Validation, and Application of PM4Sand Model in PLAXIS

Vilhar, Gregor; Laera, Anita; Foria, Federico; Gupta, Abhishek; Brinkgreve, Ronald B.J.

Citation (APA)
Vilhar, G., Laera, A., Foria, F., Gupta, A., & Brinkgreve, R. B. J. (2018). Implementation, Validation, and Application of PM4Sand Model in PLAXIS. *Geotechnical Special Publication*, *2018-June*(GSP 292), 200-211. https://doi.org/10.1061/9780784481479.021

Important note
To cite this publication, please use the final published version (if applicable).
Please check the document version above.

Implementation, validation and application of PM4Sand model in PLAXIS

Gregor Vilhar[1], Anita Laera[2], Federico Foria[3], Abhishek Gupta[4] and Ronald B.J. Brinkgreve[5]

[1]Plaxis BV, Competence Centre Geo-Engineering, P.O. Box 572, 2600 AN Delft; e-mail: gv@plaxis.com
[2]Plaxis BV, Competence Centre Geo-Engineering, P.O. Box 572, 2600 AN Delft; e-mail: al@plaxis.com
[3]Plaxis BV, Competence Centre Geo-Engineering, P.O. Box 572, 2600 AN Delft; e-mail: f.foria@plaxis.com
[4]Delft University of Technology, Delft; e-mail: a.gupta-10@student.tudelft.nl
[5]Delft University of Technology, Faculty of Civil Engineering and Geosciences, Delft; e-mail: R.B.J.Brinkgreve@tudelft.nl

ABSTRACT

This paper presents the implementation, validation and application of the PM4Sand model (version 3) formulated by Boulanger and Ziotopoulou (2015) in the PLAXIS finite element code. The model can be used for modelling geotechnical earthquake engineering applications, especially in the case liquefaction is likely to occur. The PM4Sand model represents an improvement of the elasto-plastic, stress ratio controlled, bounding surface plasticity model for sands formulated by Dafalias and Manzari (2004). The two-dimensional version has been implemented in PLAXIS and compared to the original implementation by Boulanger and Ziotopoulou (2015). The original implementation has been used in explicit finite difference simulations which can be sensitive to the size of the returned stress increment, based on the chosen time step size and loading rate. Therefore, the user needs to evaluate the sensitivity of the solution with respect to the chosen time step sizes. On the contrary, in the finite element method used here, the default time step together with the sub-stepping used at the constitutive model level, provide a robust solution independent of the size of the returned stress increment.

INTRODUCTION

The PM4Sand model is gaining popularity as a constitutive model that has been used, meanwhile, in several research projects utilising numerical nonlinear dynamic analyses, predicting the mechanical behaviour of soil and soil-structure systems subjected to earthquake loading where liquefiable sands have been involved. It is the elasto-plastic, stress-ratio-controlled, critical state compatible, bounding surface plasticity model originating from the Dafalias-Manzari model (Manzari and Dafalias 1997, Dafalias and Manzari 2004) with substantial improvements made by Boulanger (2010) and Boulanger and Ziotopoulou (2012, 2015) at UC Davis and also described in Boulanger and Ziotopoulou (2013), Ziotopoulou and Boulanger (2013), Ziotopoulou (2014).

There are many reasons why this model is a promising candidate for a wider use in the industrial projects of geotechnical earthquake engineering, among others: very accurate stress-strain and pore pressure build-up simulations under dynamic regular and irregular loading conditions, ability to accurately capture the effects of initial static shear stresses, good approximation of empirical correlations used in practice including the post-liquefaction settlements, accurate simulation of the accumulation of shear strain and strength degradation

as well as very accurate prediction of number of loading cycles to liquefaction. One of the key aspects that facilitate the wider industrial use is the very small number of material parameters that have to be calibrated by the user. Namely, the model requires only 3 primary parameters to be calibrated, while the remaining 20 parameters have predefined values that normally need no adjustment. Their values are either internally calculated from the index properties or have the default values.

In contrast to the original implementation of the PM4Sand model in a finite difference scheme, its implementation in the finite element method brings the following main advantages: a reduction of the computational time because larger load steps can be applied and an increase in the accuracy of the solution through unconditional global equilibrium of the system throughout the analysis. To be consistent with the original implementation, the model has been implemented in 2D stress conditions meaning that it can be used in plane strain analyses.

In this paper, first, the brief description of the model formulation is given. Afterwards, the undrained cyclic DSS validation results compared with the original implementation are presented for 3 different material sets corresponding to 3 different relative densities. The stress-strain, stress path, pore pressure-strain as well as $CSR - N$ plots are shown. At the end of the paper, the results of the ground response analysis of one-dimensional wave propagation are presented showing the liquefaction of the loose PM4Sand layer.

BRIEF DESCRIPTION OF THE MODEL

In this section, the main components of the model are briefly presented. For a detailed description of the formulation, the reader is referred to Boulanger and Ziotopoulou (2015). All the expressions are given in the compression positive sign convention. The bold characters indicate a tensorial quantity.

Many modifications from Boulanger and Ziotopoulou have been added to the Dafalias-Manzari model (2004) to substantially improve its simulation capabilities for geotechnical earthquake engineering applications. Among others, we can consider: revision of the fabric formation function, addition of fabric history and cumulative fabric formation terms, modification of the plastic modulus including its dependence on fabric, modification of the dilatancy expressions, splitting them into volumetric contraction and expansion parts as well as incorporating Bolton's (1986) dilatancy relation in the expansion part, modification of the elastic modulus to include dependence on stress ratio and fabric history and modification of the tracking of initial back-stress ratios. The modifications were added to improve the model behaviour in sloping ground conditions, i.e. reducing the accumulation of non-realistic shear strains as well as post-liquefaction reconsolidation. The model has also been slightly simplified by excluding the Lode's angle dependency to reduce the computation times.

In addition to the yield surface, the model uses the state dependent bounding and dilation surfaces as well as the critical state surface. In the critical state, bounding and dilatancy surfaces coincide with the critical surface. Figure 1 schematically shows all the surfaces, except the critical one, in the stress-ratio r_{yy} - r_{xy} plane. The surfaces are circular due to no Lode's angle dependency.

The state is defined via the relative state parameter index ξ_R:
$$\xi_R = D_{R,cs} - D_R$$
where D_R is the current relative density and $D_{R,cs}$ is the relative density on the critical state line at the current mean effective stress p'. Due to the 2D formulation, p' is defined as:
$$p' = \frac{\sigma'_h + \sigma'_v}{2}$$

where σ'_h and σ'_v are the effective horizontal and vertical stresses, respectively. The critical state line is a function of the Bolton's (1986) Q and R parameters and the atmospheric pressure p_A:

$$D_{R,cs} = \frac{R}{Q - \ln(100\frac{p'}{p_A})}$$
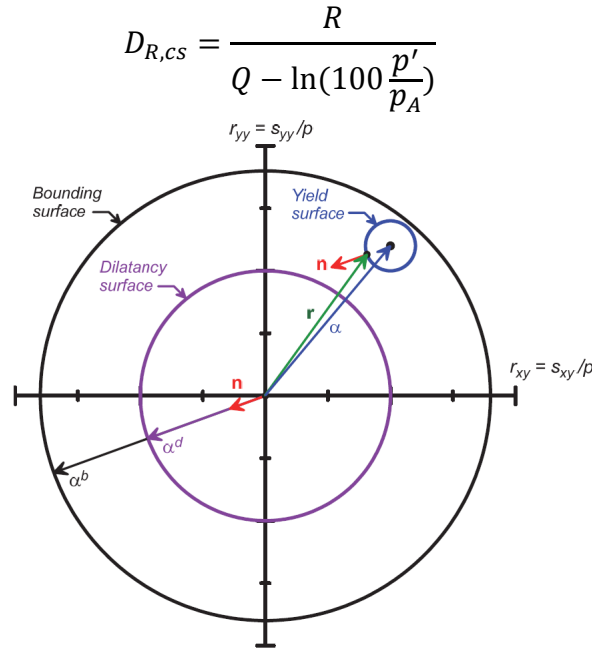
Figure 1. Yield, dilatancy and bounding surfaces in the stress-ratio r_{yy} - r_{xy} plane together with the corresponding normal tensor (Boulanger and Ziotopoulou, 2015).

The bounding surface ratio M^b and the dilation surface ratio M^d are defined as:

$$M^b = M \exp(-n^b \xi_R)$$
$$M^d = M \exp(n^d \xi_R)$$

where n^b and n^d are material parameters and M is the critical surface ratio defined by the critical state friction angle φ_{cv} as:

$$M = 2\sin(\varphi_{cv})$$

Using the ratios M^b and M^d, the image back-stress ratio tensors for bounding and dilation surfaces $\boldsymbol{\alpha}^b$ and $\boldsymbol{\alpha}^d$ are expressed as:

$$\boldsymbol{\alpha}^b = \sqrt{\frac{1}{2}}[M^b - M]\,\boldsymbol{n}$$

$$\boldsymbol{\alpha}^d = \sqrt{\frac{1}{2}}[M^d - M]\,\boldsymbol{n}$$

where $\boldsymbol{n}$ is the normal to the yield surface. Additionally, M^d is scaled to get the rotated dilatancy surface which is active when fabric is unfavourable. Initial back stress ratio $\boldsymbol{\alpha}_{in}$ is tracked according to bounding surface formulation of Dafalias (1986). In order to avoid the over-stiffening at stress reversals, $\boldsymbol{\alpha}_{in}$ is subdivided into apparent $\boldsymbol{\alpha}_{in}^{app}$ and true $\boldsymbol{\alpha}_{in}^{true}$ initial back stress ratios. Additionally, the previous initial back stress ratio $\boldsymbol{\alpha}_{in}^{p}$ is tracked. Together with the state, stress and fabric evolution terms, the distances from the yield surface back-stress ratio $\boldsymbol{\alpha}$ to $\boldsymbol{\alpha}^b$, $\boldsymbol{\alpha}^d$ and $\boldsymbol{\alpha}_{in}$ form the dilatancy (D) and plastic modulus (K_p) expressions. The complex expressions and conditions needed to compute D and K_p are not given in this paper due to brevity. The non-associated flow rule used by the model is defined as:

$$d\boldsymbol{\varepsilon}^p = \langle L \rangle (\boldsymbol{n} + \frac{1}{3}D\boldsymbol{I})$$

where $d\boldsymbol{\varepsilon}^p$ is the plastic strain increment, $\langle\,\rangle$ MacCauley brackets, L is the plastic multiplier and $\boldsymbol{I}$ the identity matrix. The movement of the axis of the yield surface is given by the kinematic hardening rule:

$$d\boldsymbol{\alpha} = \langle L \rangle \frac{2}{3} h \left(\boldsymbol{\alpha}^b - \boldsymbol{\alpha}\right)$$

where h is defined as:

$$h = \frac{3}{2} \frac{K_p}{p'(\boldsymbol{\alpha}^b - \boldsymbol{\alpha}):\boldsymbol{n}}$$

and the symbol : denotes the trace of the product of adjacent tensors, i.e. $\boldsymbol{a}:\boldsymbol{b} = tr(\boldsymbol{ab})$. The effects of strain history are taken into account by using the fabric-dilatancy tensor $\boldsymbol{z}$ defined by Dafalias and Manzari (2004). The evolution of $\boldsymbol{z}$ is expressed by the following formula:

$$d\boldsymbol{z} = -\frac{c_z}{1 + \langle\frac{z_{cum}}{2\,z_{max}} - 1\rangle} \frac{\langle -d\varepsilon_v^{pl}\rangle}{D} (z_{max}\boldsymbol{n} + \boldsymbol{z})$$

where $d\varepsilon_v^{pl}$ is the volumetric strain increment, z_{cum} the sum of norms of changes in $\boldsymbol{z}$, z_{max} the parameter denoting the maximum value that $\boldsymbol{z}$ can attain and c_z being the parameter controlling the rate of evolution of $\boldsymbol{z}$.

The non-linear elastic part of the model is a function of the constant Poisson's ratio ν as well as the stress, stress-ratio and fabric dependent shear modulus G:

$$G = G_0 p_A \left(\frac{p}{p_A}\right)^{\frac{1}{2}} C_{SR} \left(\frac{1 + \frac{z_{cum}}{z_{max}}}{1 + \frac{z_{cum}}{z_{max}} C_{GD}}\right)$$

where the shear modulus coefficient G_0 is a constant, C_{SR} is a factor that accounts for stress ratio effects and C_{GD} is a parameter that describes the effect of the degradation of G at very large values of z_{cum}.

VALIDATION OF THE MODEL IMPLEMENTATION IN CYCLIC SINGLE ELEMENT SIMULATIONS

In order to validate the implementation of the model in PLAXIS, many single Gauss point and single element monotonic and cyclic tests were performed. Herein, the results of a series of single element undrained cyclic direct simple shear test simulations are shown. The chosen relative densities of simulations are $D_R = 35\%$, 55% and 75% in accordance with the published values of the report by Boulanger and Ziotopoulou (2015). D_R represents also one of the three primary parameters of the model. The other two, namely the shear modulus coefficient G_0 and the contraction rate parameter h_{p0} are assigned consistently with the report (Table 1). In order to determine G_0, the simplified expression for a range of typical densities and stress levels, given in Boulanger and Ziotopoulou (2015) is used to calibrate the material in this paper:

$$G_0 = 167 \sqrt{(N_1)_{60} + 2.5}$$

where the values of $(N_1)_{60}$, normalised penetration resistance for SPT, were calculated by using the expression by Idriss and Boulanger (2008):

$$D_R = \sqrt{\frac{(N_1)_{60}}{46}} \quad (1)$$

Alternatively, the elastic shear modulus G can be calculated based on correlations between the shear wave velocity V_{s1} and the penetration resistance. Similar values of G_0 can then be derived using the following expression:

$$G = G_0 p_A \left(\frac{p}{p_A}\right)^{\frac{1}{2}}$$

The parameter h_{p0} in the dilatancy expression controls the contractiveness of the model response. It enables the calibration of the model to specific cyclic resistance ratios (CRR). The target values of CRR for an effective overburden stress of 1 atm and an earthquake magnitude of $M = 7.5$ were selected from Idriss and Boulanger (2008) $CSR - (N_1)_{60}$ correlation. An SPT-based estimate of CRR for an earthquake of $M = 7.5$ and 1 atm effective overburden stress was assumed by the authors of the report to be approximately equal to the CRR value at 15 uniform loading cycles causing a peak shear strain of 3% in DSS loading.

The other parameters of the model can be considered as secondary parameters for which the default values have been used as recommended by the authors of the model. In Table 1 the values of primary parameters are given for 3 parameter sets as well as corresponding in-situ conditions that were derived from the published correlations.

Table 1. In-situ conditions and values of primary parameter sets used in performed DSS simulations, a) Eq.1, b) Andrus and Stokoe, 2000, c) Idriss and Boulanger, 2008.

Set	In-situ conditions from published correlations				Model parameters		
	D_R [-]	$(N_1)_{60}$ [-] (a)	V_{S1} [m/s] (b)	$CRR_{M=7.5}$ (c)	D_R [-]	G_0 [-]	h_{p0} [-]
1	0.35	6	139	0.090	0.35	476	0.53
2	0.55	14	171	0.147	0.55	677	0.40
3	0.75	26	198	0.312	0.75	890	0.63

In Figure 2, the comparison between the simulated and published data regarding the cyclic stress ratio versus the number of uniform cycles to cause liquefaction defined as 1%, 3% and 7.5% single amplitude shear strain is shown.
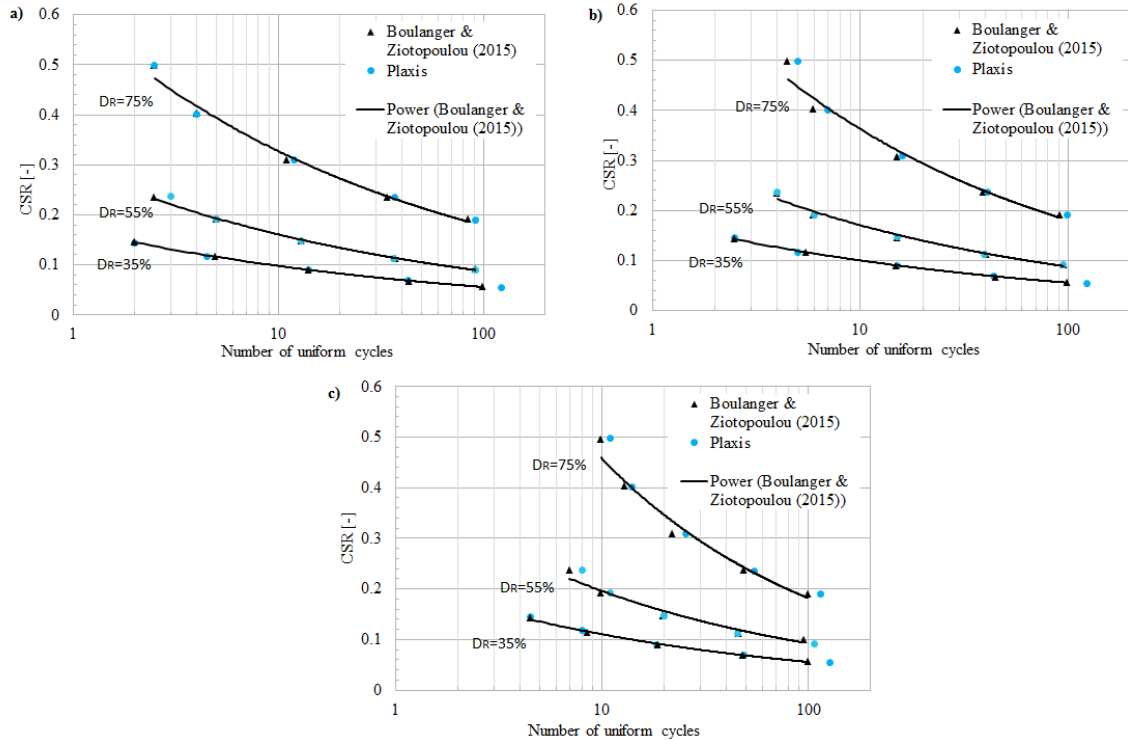
Figure 2. Cyclic stress ratios (CSR) versus the number of uniform loading cycles to cause liquefaction defined as a single amplitude shear strain reaching (a) 1%, (b) 3% and (c) 7.5% in undrained DSS simulations at σ'$_{v0}$ = 100kPa.

It can be observed that the number of cycles to liquefaction calculated with the PLAXIS implementation of the model is very close to the published results. The differences are within the acceptable tolerance for engineering applications. Nevertheless, our future efforts will be focused on further approaching the trends of the original implementation.

Figures 3 show plots of $\tau_{xy} - \gamma_{xy}$ (3a, 3d, 3g), $\tau_{xy} - \sigma_v'$ (3b, 3e, 3h) and $pwp - \gamma_{xy}$ (3c, 3f, 3i) for single element undrained cyclic DSS tests performed with 3 different material sets (Table 1) and 3 different cyclic stress ratios. The results are compared with the original implementation of the model. Also in these figures, it can be observed that the PLAXIS model simulations are very close to the simulations of the original model implementation. The differences are also in this case within the acceptable tolerance for engineering applications.
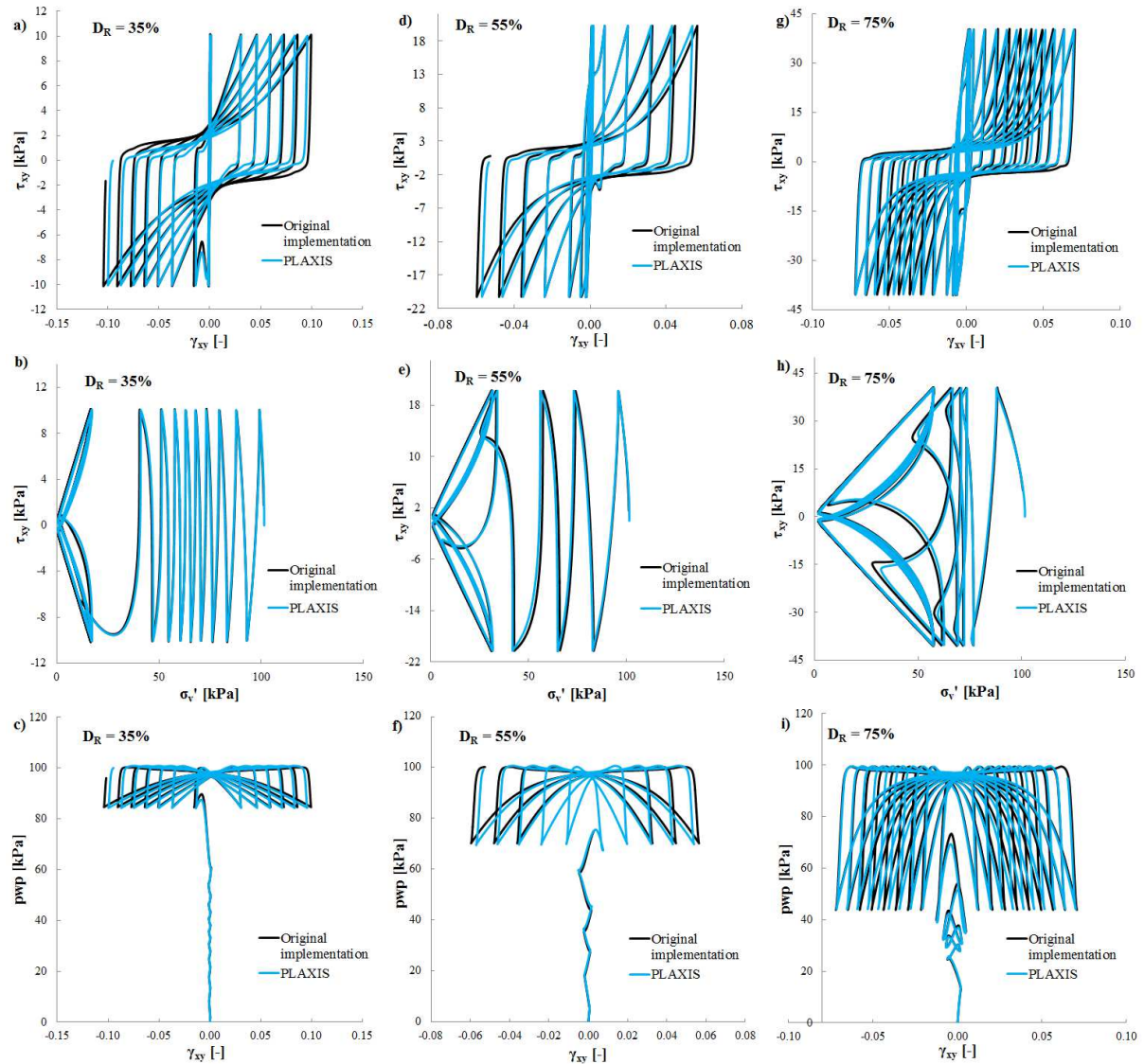
Figure 3. Plots of $\tau_{xy} - \gamma_{xy}$, $\tau_{xy} - \sigma_v'$ and $pwp - \gamma_{xy}$ showing the comparison between simulation of undrained cyclic stress-controlled DSS tests with the original implementation using the parameter set 1 and CSR = 0.1 (a), (b) and (c), parameter set 2 and CSR = 0.2 (d), (e) and (f), parameter set 3 and and CSR = 0.4 (g), (h) and (i). In all cases, $\sigma_{v0}' = 100$kPa and $K_0 = 0.5$.

Figure 4 shows the comparison of the overburden correction factor K_σ between the empirical relations recommended by Boulanger and Idriss (2004), original implementation simulations (black markers) and our implementation simulations (blue markers). It can be

seen that there are very small differences between the original and our implementation for $D_R=35\%$ while the values for $D_R=55\%$ and $D_R=75\%$ coincide.
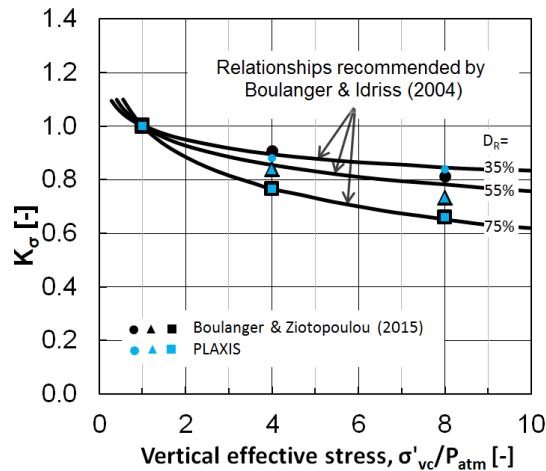
Figure 4. K_σ factors determined at 15 uniform loading cycles to cause 3% single-amplitude shear strain (modified from Boulanger and Ziotopoulou, 2015).

APPLICATION OF THE MODEL IN ONE-DIMENSIONAL SITE RESPONSE ANALYSIS

In order to further test the simulation capabilities of the PM4Sand model implemented in PLAXIS, a 1D wave propagation analysis was performed. The aim of the analysis was to verify that the PM4Sand model is able to predict the onset of liquefaction in sandy layers. The soil stratigraphy consisted of an overconsolidated clay layer of medium compressibility that extended from the ground surface to 5m depth, followed by 10m of sand layer and 25m of clay (Figure 5), until the bedrock was reached. The water table was assumed to be coincident with the ground surface level. The clay material was modelled using the HS small constitutive model (Benz, 2006), while the PM4Sand model was used to simulate the behaviour of the sand. The material parameters of the clay and sand layers are given in Tables 2 and 3, respectively. For both materials, the behaviour was considered undrained and the Rayleigh damping coefficients α and β were assumed equal to 0.096 and 0.00079 (based on the target damping ratio ξ equal to 1% in the frequency range between 1.03 and 3 Hz, following the strategy proposed by Hudson, Idriss & Beirkae (1994)).

Table 2. HS small parameters of clay

Parameter	Symbol	Value	Unit
Saturated unit weight	γ_{sat}	21	kN/m^3
Unsaturated unit weight	γ_{unsat}	19	kN/m^3
Secant stiffness in standard drained TX test	E_{50}^{ref}	9000	kN/m^2
Tangent stiffness for primary oedometer loading	E_{oed}^{ref}	9000	kN/m^2
Unloading-reloading stiffness	E_{ur}^{ref}	27000	kN/m^2
Power for stress-level dependency of stiffness	m	1	-
Shear modulus at very small strains	G_0^{ref}	60000	kN/m^2
Shear strain at which $G_s = 0.722\ G_0$	$\gamma_{0.7}$	0.0007	-
Friction angle	φ'	26	°
Cohesion	c_{ref}'	30	kN/m^2

Dilatancy angle	ψ	0	$^\circ$
Failure ratio	R_f	0.9	-
Poisson's ratio	v_{ur}'	0.2	-
Tensile strength	σ_t	0	kN/m^2
Reference stress	p_{ref}	100	kN/m^2
Over-consolidation ratio	OCR	2	-
Earth pressure coefficient	K_0	0.87	-

Table 3. PM4Sand parameters of sand

Parameter	Symbol	Value	Unit
Saturated unit weight	γ_{sat}	18	kN/m^3
Unsaturated unit weight	γ_{unsat}	14	kN/m^3
Relative density	D_R	55	%
Shear modulus coefficient	G_0	677	-
Contraction rate	h_{p0}	0.40	-

The bedrock layer of 1m thickness was modelled with the linear elastic material of drained type behaviour. γ_{sat} and γ_{unsat} were set to $22 kN/m^3$. The Young's modulus and Poisson's ratio were set to $8 \cdot 10^6$ kN/m^2 and 0.2, respectively.

The Loma Prieta 1989 accelerogram was used as input ground motion. It is characterised by a moment magnitude M_w equal to 6.9. The input signal was scaled at a peak horizontal acceleration of $0.3g$. The earthquake was assumed to be measured at the outcrop of a rock formation and was modelled by imposing a prescribed displacement at the bottom of the model. The boundary condition at the base of the model was defined using a compliant base. The vertical boundaries were modelled with tied degrees of freedom, which allow to simulate the one-dimensional behaviour in a 2D soil column.

Figure 5 shows the finite element mesh of the model with prescribed displacements at the bottom and the time history acceleration of the imposed earthquake signal.
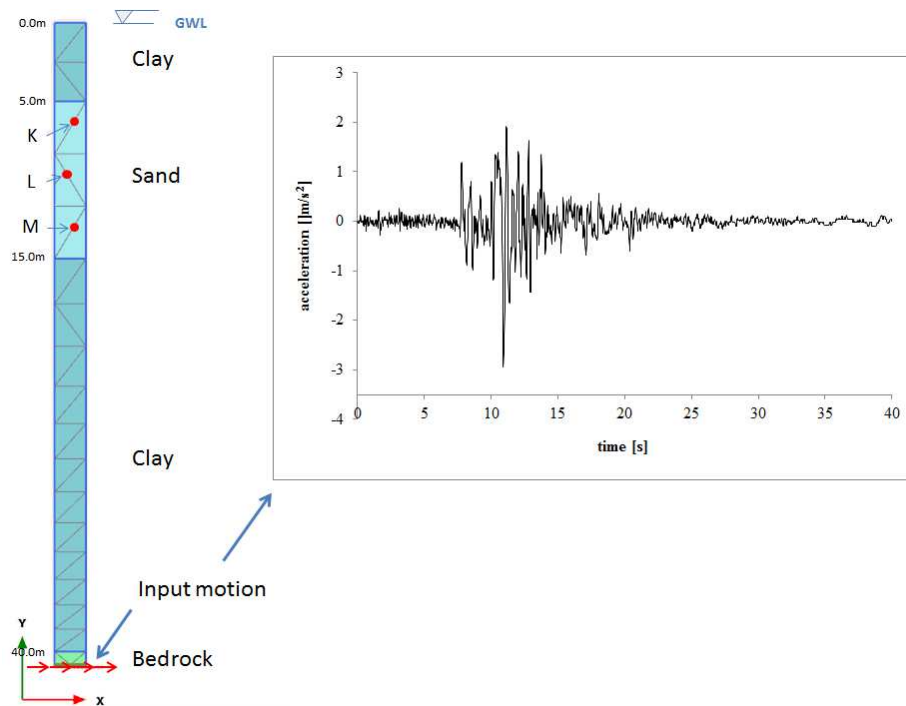
Figure 5. Connectivity plot of the numerical model and time history acceleration of the earthquake motion.

Figure 6 shows the results at the end of the analysis. It can be seen that the maximum excess pore pressure ratio $r_{u,max}$ is between 0.9 and 1 (6a), i.e. the sand layer has completely liquefied. The evolution of the excess pore pressure ratio r_u with time for the points K, L and M in the sand layer (6b) shows that after 13s of dynamic loading the excess pore pressure ratio r_u is greater than 0.93 in all the three points.
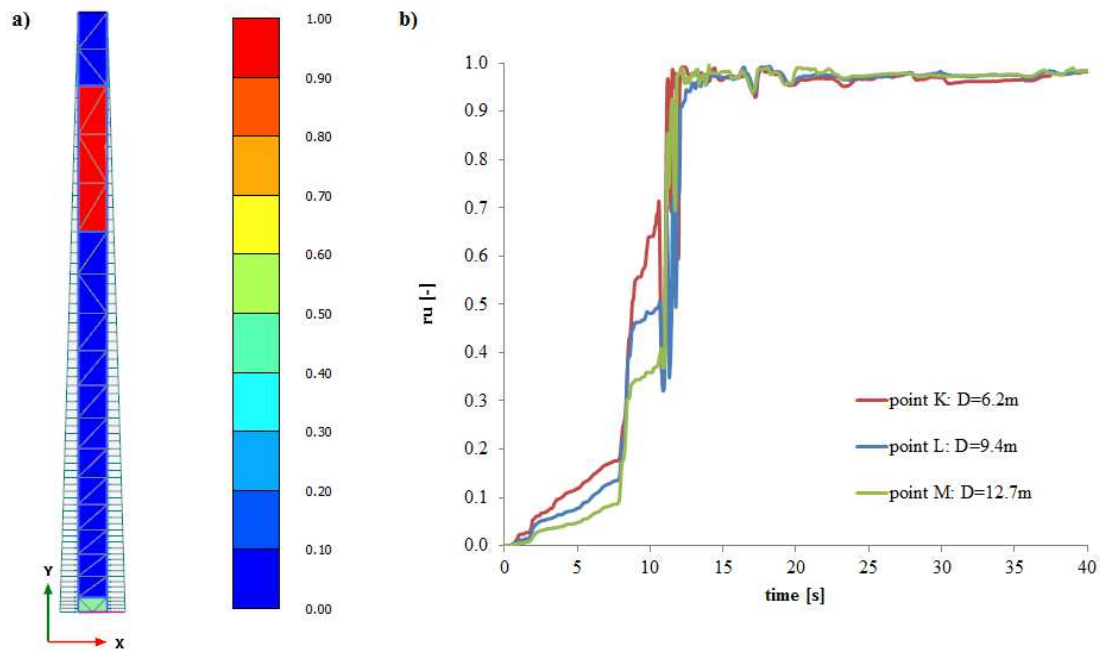
Figure 6. Maximum excess pore pressure ratio r_{u,max} at the end of the dynamic analysis (a) and excess pore pressure ratio r_u for points K, L and M during the dynamic calculation (b).

CONCLUSIONS

The implementation, validation and practical application of the PM4Sand model (version 3) by Boulanger and Ziotopoulou (2015) in the PLAXIS finite element code has been presented in this paper. The implementation of the model has been validated by comparing the $CSR - N$ graphs from cyclic undrained single element direct simple shear simulations with the original implementation of the model. Moreover, $\tau_{xy} - \gamma_{xy}$, $\tau_{xy} - \sigma_v'$ and $pwp - \gamma_{xy}$ comparisons are shown in the paper for 3 material sets with 3 different cyclic stress ratios. The results show a very good agreement with the original implementation of the model. The implemented model was also used for an application, i.e. a one-dimensional site response analysis. The behaviour of the loose sand layer was simulated with the PM4Sand model while the clay layers were modelled with the HS small model. The results show that the loose sand layer completely liquefies under the applied earthquake loading of magnitude $M = 6.9$. The model is capable of modelling the accumulation of excess pore pressures and triggering liquefaction in saturated loose sands subjected to cyclic loading.

According to the performed validations and applications of the model, it can be concluded that the PM4Sand model has successfully been implemented into the PLAXIS finite element code.

REFERENCES

Andrus, R.D., and Stokoe, K.H. (2000). "Liquefaction resistance of soils from shear-wave velocity." *J. Geotechnical and Geoenvironmental Eng.*, ASCE 126(11), 1015–025.

Benz, T. (2006). Small-Strain Stiffness of Soils and its Numerical Consequences. Ph.d. thesis, Universität Stuttgart.

Bolton, M.D. (1986). The strength and dilatancy of sands. Geotechnique, 36 (1): 65-78

Boulanger, R. W. (2010). "A sand plasticity model for earthquake engineering applications." *Report No. UCD/CGM-10-01*, Center for Geotechnical Modeling, Department of Civil and Environmental Engineering, University of California, Davis, CA, 77 pp.

Boulanger, R. W., and Idriss, I. M. (2004). "State normalization of penetration resistances and the effect of overburden stress on liquefaction resistance. *Proc., 11th Intl. Conf. on Soil Dynamics and Earthquake Engineering, and 3rd Intl. Conf. on Earthquake Geotechnical Engineering*, Doolin et al., eds, Stallion Press, Vol. 2, pp. 484-491.

Boulanger, R. W., and Ziotopoulou, K. (2012). "A sand plasticity model for earthquake engineering applications: Version 2.0." *Report No. UCD/CGM-12/01*, Center for Geotechnical Modeling, Department of Civil and Environmental Engineering, University of California, Davis, CA, 100 pp.

Boulanger, R. W., and Ziotopoulou, K. (2013). "Formulation of a sand plasticity plane-strain model for earthquake engineering applications." *Journal of Soil Dynamics and Earthquake Engineering*, Elsevier, 53, 254-267, 10.1016/j.soildyn.2013.07.006.

Boulanger, R.W. and Ziotopoulou, K. PM4Sand (Version 3) (2015). "A Sand Plasticity Model for Earthquake Engineering Applications". *Report No. UCD/CGM-15/01*, Center for Geotechnical Modeling, Department of Civil and Environmental Engineering, Univ. of California, Davis, CA; 108 pp.

Dafalias, Y. F. (1986). "Bounding surface plasticity. I: Mathematical foundation and hypoplasticity." *J. Engineering Mechanics*, 112(9), 966-987.

Dafalias, Y. F., and Manzari, M. T. (2004). "Simple plasticity sand model accounting for fabric change effects." *Journal of Engineering Mechanics*, ASCE, 130(6), 622-634.

Hudson, M., Idriss, I. and Beirkae, M. (1994). Quad4m user's manual.

Idriss, I. M., and Boulanger, R. W. (2008). "Soil liquefaction during earthquakes". *Monograph MNO-12*, Earthquake Engineering Research Institute, Oakland, CA, 261 pp.

Manzari, M. T., and Dafalias, Y. F. (1997). "A critical state two-surface plasticity model for sand." *Géotechnique*, 47(2), 255-272.

Ziotopoulou, K., and Boulanger, R. W. (2013). "Calibration and implementation of a sand plasticity plane-strain model for earthquake engineering applications." *Journal of Soil Dynamics and Earthquake Engineering*, 53, 268-280.

Ziotopoulou, K. (2014). "A sand plasticity model for earthquake engineering applications." *PhD Dissertation*, University of California, Davis.